2D Imaging of a Helicon Discharge

David D. Blackwell Francis F. Chen

Electrical Engineering Department

PPG- 1571 revised September, 1997

2D IMAGING OF A HELICON DISCHARGE

David D. Blackwell and Francis F. Chen

Electrical Engineering Department, University of California, Los Angeles, California 90095-1594

Two-dimensional images of the ionized argon light of a helicon discharge are made both along and across the magnetic field with various antenna configurations. Two antennas, a Nagoya Type III and a helical antenna, are used to create a magnetized RF plasma with density in the range $n \leq 5 \times 10^{13}$ cm^{-3}. A CCD camera with a 488nm bandpass filter is used to image the plasma as magnetic field and power are changed. By inserting a Faraday shield, it is demonstrated that the inductive component of the antenna coupling is responsible for producing high density plasmas. Asymmetries in the plasma profile are shown to be caused primarily by capacitive coupling, with the purely inductively coupled plasmas being symmetric and centrally peaked. Numerical calculations of antenna coupling show that the configurations having the largest antenna loading correspond to the brightest plasmas observed in the experiment, with the m = +1 mode being the most strongly coupled.

I. INTRODUCTION

Over the past decade there has been increasing interest in helicon wave discharges because they have been shown [1-7] to produce high density plasmas ($n > 10^{12}$ cm^{-3}) with relatively small amounts of RF power ($P_{rf} \leq 3$kW). Theoretical treatments [8,9] of this discharge have been done using the well developed theory of waves in a bounded plasma, giving several scaling laws to which experimental data are fit. Unfortunately, many observations have been made [10,11] which are not easily explained, and clearly depend at least partially on antenna coupling. Only recently [12-15] have complete numerical methods been developed to properly solve the problem of antenna coupling, allowing a more realistic comparison of theory and experiment to be made.

With a view toward such experiments, we examine in this paper the experimental conditions required to match the assumptions in the theories. In particular, we can observe the effect of capacitive coupling, which is usually neglected in theory, by inserting a Faraday shield between the antenna and the glass chamber. It is shown that even in high density regimes where the plasma has been referred to as "wave coupled" [10], capacitive coupling can have a significant effect on the plasma properties. Most apparent was the effect of this coupling on the plasma profile, which shows that using simple helicon wave theory to explain the observed profiles [16] is in most cases unsatisfactory. We show that previously observed jumps in density [5] as the magnetic field or RF power is raised cannot be described simply by the density on axis. The entire density profile changes at the jumps. A second important parameter is antenna geometry. In previous experiments, more than one antenna configuration is used [3,6,11], but until now the antenna coupling calculations were not easily

available, so that interpretation of results could only be qualitative. Here, we compare our observations with the results from a numerical code which solves the problem of antenna coupling to a nonuniform plasma [15]. Specifically, we show that an $m = +1$ helical antenna yields a higher density plasma than a straight Nagoya Type III antenna, in agreement with the predictions of the code. This agreement, along with the effects of eliminating the capacitive coupling, demonstrates that the inductive coupling of the antenna to helicon waves is responsible for producing high plasma densities.

II. APPARATUS

The plasma was created in a 108 cm long, 10-cm diam pyrex chamber (Fig. 1), which is evacuated to a base pressure $p \leq 3\text{x}10^{-6}$ Torr and surrounded by eight 25-cm diam coils which produce a magnetic field in the range 350-1000G. The center of the antenna is located approximately 25 cm from the axial midplane of the chamber, at which point there are two ports located 90° azimuthally from each other. One port is for a Langmuir probe, and the other is used for the gas feed and pressure monitors. The antenna is driven with $P_{rf} \leq 2$kW of RF power at 13.56 MHz in 50-msec pulses about 4 sec apart. A standard L-type capacitive tuning circuit is used to match the power supply to the antenna, and the incident and reflected powers are monitored with in-line power meters between the RF amplifier and tuning circuit. Fig. 2 shows the antennas used. The Nagoya Type III antenna, Fig. 2a, was 11 cm in diam by 20 cm long, and the helical antenna, Fig. 2b, was 11 cm in diam by 16 cm long.

The end of the chamber nearer the antenna is sealed by a 10-cm diam glass window to allow viewing of the plasma along the axis of the chamber. A Cohu Electronics type RS-170 CCD camera is positioned either in front of this window or at one of the three side ports (see Fig. 1) for transverse viewing. A bandpass optical filter with a central wavelength of 488 nm and a half-bandwidth of 10 nm is placed in front of the camera so that the only light collected is from Ar^+ emission, which is proportional to the square of the plasma density. The camera is focused at either the axial or radial center of the chamber depending on its viewing direction. The camera has a shutter speed of 1/60 sec and is triggered 20 ms after the RF pulse, when the plasma has reached steady-state conditions.

As will be discussed in Sec. IV, the 488-nm light intensity is proportional to $n^2\langle sv\rangle$, where n is the plasma density and $\langle sv\rangle$ a steep function of electron temperature T_e. No RF-compensated probes were available this time for measuring T_e, but 2.5-3.5 eV temperatures had been measured in a previous experiment on the same apparatus. To calculate n from ion saturation currents, an average temperature of 3 eV was used. The two-dimensional patterns seen with the CCD camera were therefore caused by a convolution of T_e and n variations, but these could not be separated because a 2D Langmuir probe drive was not available.

III. RESULTS

1. Nagoya Type III antenna

The plasma density inferred from measurements of the ion saturation current versus input power P_{rf} and magnetic field B_0 is shown in Figs. 3a and 3b, respectively. The matching circuit was carefully retuned at each setting. These curves show more gentle "jumps" as P_{rf} and B_0 are raised than have been reported by others [5, 7]. In the largest jump seen here, between 490 and 540 G in Fig. 3b, the plasma density increases by more than 40%. The

emission profile viewed along the cylindrical axis showed that during this increase the plasma was making a transition from being localized at two positions off-axis to being somewhat bean-shaped, with a higher concentration of light in the center of the chamber (Figs. 4a and 4b). In both cases, the discharge is azimuthally asymmetric. At the highest magnetic field of 740 Gauss, the plasma was observed to be concentrated along a line between the straight segments of the antenna, as seen in Fig. 5. Initially one could be inclined to think that these asymmetries were caused by the fact that the peak energy deposition for helicon waves is centered off axis [3], so that such a pattern of light could be explained perhaps by a plane-polarized wave excited by the antenna. To verify whether this distribution of light was due to a wave phenomenon, a Faraday shield was installed between the antenna and the glass chamber. The Faraday shield was a simple aluminum sheet with slots cut longitudinally and transversely as shown in Fig. 6. This will shield the plasma from the electrostatic field generated by the high voltages on the antenna but will allow the electromagnetic fields generated by the antenna currents to pass through. After it was put in place, its effectiveness was tested using a capacitive probe designed similarly to that described in [17] to verify that the vacuum electrostatic field was indeed being blocked. The electromagnetic field was also measured before and after installation in a similar manner using a magnetic loop probe as described in [6] to establish that that component of the field was minimally shielded.

With the shield installed, there were major differences in the discharge operation. The most noticeable was that the plasma emission profile was radically changed, becoming much more symmetric and centralized. This is demonstrated in Fig. 7, where the plasma image with the shield can be compared to the unshielded case of Fig. 4. In fact, the sharp increase in density that was seen earlier in the range of 500 G was no longer present once the shield was installed, as shown in Fig. 8. Also gone was the change in the plasma emission profile that accompanied this increase. However, a large drop in density now appears as the input power is reduced, an effect not observed when the antenna was unshielded. Figure 9 shows that during this drop the plasma profile is again making a transition, this time from being centrally peaked to being edge-localized. The asymmetry seen in Fig. 9 can be related to the location of the gap in the Faraday shield.

2. Helical antenna

Figures 10a and 10b show that, for the same values of power and magnetic field, the helical antenna always produces a higher peak plasma density than does the Nagoya Type III. In addition, the emission profile for these discharges was always very symmetric azimuthally, as shown in Fig. 11. This is not surprising, since the axial views are integrated over z, and the antenna has no preferred azimuth. The addition of the same Faraday shield used in our Nagoya-antenna measurements did nothing to change this profile, but did cause a density drop at low P_{rf} similar to what we observed with the Nagoya antenna. This is shown in Fig. 12. Again, during this density drop the plasma profile changed from its normally very centrally peaked profile to an edge-localized profile similar to that of Fig. 9. Although the insertion of the Faraday shield did not change the symmetry of the discharge with the helical antenna, it did have the unexpected effect of decreasing the peak density by about a factor of two, as seen in Figs. 12a and 12b. This could have been caused by partial shielding of the inductive field by currents in the Faraday shield that could flow around the single insulating gap. This simple shield was used because of the difficulty in eliminating ground loops and obtaining proper RF grounding. In fact, to obtain approximate settings for the tuning capacitors with

the shield installed, it was necessary to inject electrons with an electron gun in order to obtain breakdown.

Another difference between the two antennas was that the plasma produced by the helical antenna was sensitive to one additional parameter: the direction of the magnetic field. Figure 13 shows transverse images of the plasma viewed at three axial positions for the three antenna configurations. Note that the plasmas produced by the helical antenna again are seen to have a distinct center compared with the broad plasma produced by the Nagoya antenna. In the region farthest from the antenna, we see that the helical plasma with clockwise helicity relative to the magnetic field maintains its intensity and central structure. When the direction of the magnetic field is reversed, the plasma decays much more rapidly.

IV. INTERPRETATION OF RESULTS

The optical emission at 488 nm can come from electron collisions with Ar I neutrals or with Ar II ions. Because of the higher threshold for direct excitation from Ar I, one would expect this process to be negligible. Indeed, in a previous paper Sudit and Chen [18] showed that data on the axial variation of 488-nm light agreed with calculations, based on measured T_e's, assuming the n^2 dependence of the Ar II process but not with the n dependence of the Ar I process. Thus, the light intensity in our CCD images should be proportional to $n^2\langle sv\rangle$. The cross section s for excitation of the 488-nm line by electron impact on Ar^+ ions was measured by Imre et al. [19] and is shown in Fig. 16. Integrating this over a Maxwellian distribution gives the curve of $\langle sv\rangle$ vs. T_e shown by the dashed line in Fig. 17. Though this is a steep function of T_e, the latter varies little across the plasma because electron thermal diffusivity is large even across the magnetic field, a manifestation of what is commonly known as "Langmuir's paradox". This is shown by data taken with a fully RF-compensated probe [20] in another helicon experiment on the same apparatus under similar conditions. Fig. 18 shows radial profiles of T_e at 1kW of RF power, 6 mTorr of Ar, and various magnetic fields. The central densities are in the range $1.2\text{-}1.6 \times 10^{13}$ cm^{-3}. It is seen that the profiles are nearly flat within the expected experimental error of ±0.2 eV, with no systematic radial variation. The slight rise in T_e at the edge is probably caused by the failure of RF compensation at densities below 10^{13} cm^{-3}. The change in $\langle sv\rangle$ when T_e varies from 2.5 to 3.5 eV is shown by the shaded portion of the $\langle sv\rangle$ curve in Fig. 17 and amounts to a little more than an order of magnitude. By comparison, the variation in the n^2 factor is shown in Fig. 17 as the solid curve, and this also varies by a little more than an order of magnitude as n varies from 1 to 5×10^{13} cm^{-3}, as it does in the density data given in this paper. Thus, the light patterns are attributable to both T_e and n variations during jumps from capacitive coupling to inductive coupling and finally to helicon wave generation.

Because of the 17-eV threshold in Fig. 16, optical emission is extremely sensitive to high energy tails in the electron distribution. If such hyperthermal electrons exist in large numbers, they would be responsible for the observed light patterns. Our conclusions that the plasma changes in a two-dimensional manner when abrupt jumps in axial density are observed or when Faraday shields are installed are nonetheless valid. We do not believe, however, that hyperthermal electrons abound in helicon discharges at densities well above 10^{13} cm^{-3}. In a previous experiment [21], a carefully RF-calibrated gridded energy analyzer was used, and no electron tails could be seen down to the measurement limit of 1%.

V. DISCUSSION

From the images of the plasma observed with and without the Faraday shield installed, it is clear that the asymmetries observed in the light emission profile cannot be solely attributed to wave coupling phenomena. Even at very high densities and magnetic field strengths, where the discharge has been described as being primarily wave driven, Figs. 8 and 12 demonstrate that a significant amount of power is capacitively coupled. Although it is likely that the inductive coupling is the process responsible for the most of the heating of the higher density plasmas, a complete picture of the power deposition and antenna coupling must include both components.

Recall that there was an abrupt decrease in plasma density and a transition in the emission profile that occurs in the range of 500 W when the antennas were shielded. This can be explained as follows. When the antenna is initially turned on, capacitive coupling is needed to provide initial breakdown of the gas. Once a plasma has developed, the inductive fields can heat it, and the density will rapidly increase. There is a minimum initial density required for this inductive heating to be effective.

This minimum density is a consequence of the fact that the inductive fields have a spatial structure and dispersion relation imposed on them by the plasma. These are what are referred to as the plasma eigenmodes. Because of these eigenmodes, only a fraction of the inductive fields of the antenna have the correct structure to be supported by the plasma. The larger this fraction is, the more inductive power can be utilized to heat the plasma. This is why the antenna geometry is important and why the helical antenna is better coupled than the Nagoya Type III.

A rigorous treatment of this problem has been done by Shamrai [13], in which he calculates the linear response of a uniform plasma to an external antenna current. More recently Arnush [15] has generalized this calculation to a nonuniform plasma. In both calculations the amplitude of the induced fields in the plasma is found to be related to the Fourier transform of the antenna current by

$$\Psi_i = F_i(r,m,k)\,J_j\,(m,k) \tag{1}$$

Here Ψ_i is the amplitude of a field component (**E** or **B**), F_i is a function of the plasma parameters (e.g., density, magnetic field, and radial profile), and J_φ is the Fourier transform of the antenna surface current, defined as

$$J_j\,(m,k) = \frac{1}{2p}\int_{-\infty}^{\infty} dz \int_0^{2p} dj\;\; J_j\,(j\,,z)e^{-i(mj+kz)} \tag{2}$$

For the helical antenna, this term is

$$J_j\,(m,k) = \frac{k}{mp}\,\frac{\sin(\tfrac{1}{2}kL - mq)}{\tfrac{1}{2}kL - mq} \tag{3}$$

while for the Nagoya Type III antenna it is

$$J_j\,(m,k) = \frac{2}{mp}\sin\left(\frac{kL}{2}\right) \tag{4}$$

Here L is the length of the antenna, m is the azimuthal mode number, and q is the pitch angle of the helix for the helical antenna. Figure 14 shows that the spectrum of the helical antenna is narrower and has a larger amplitude than that of the Nagoya Type III antenna for the lowest

azimuthal modes $m = \pm 1$. In addition, as shown in Ref. [15], the plasma response is invariant to reversing the sign of k but not to reversing the sign of m, so that the azimuthal mode content will be generally be more heavily weighted towards either clockwise or counterclockwise polarization. Experimentally, this was demonstrated in Fig. 13 by reversing the magnetic field, which amounts to changing k to $-k$ in Eq. (3). The spectral power density for each antenna was calculated numerically by solving the boundary value problem as outlined by Arnush [15]. This can be expressed as the antenna loading resistance, where the resistance is related to the inductive power deposited by Ohm's Law:

$$P = \tfrac{1}{2} I_a^2 R \tag{5}$$

where I_a is the antenna current. The higher the resistance, the more efficient the antenna configuration, since the same amplitude waves can be driven using a smaller amount of current. In practice the total load to the powers supply will also include losses in the circuit and capacitive loading, so that the total power used will be

$$P = \tfrac{1}{2} I_a^2 (R_i + R_c + R_s), \tag{6}$$

with R_i representing the inductive (wave) loading, R_c the non-inductive (capacitive) loading, and R_s the stray losses in the circuit. Experimentally, the best helicon wave coupling is obtained by designing the antenna with R_i as large as possible. Figure 15 shows the loading resistance per wavenumber, with the integrated area under each curve representing the total loading resistance R. We can see that the loading spectrum for the helical antenna is not only much narrower for the $m = +1$ mode, but the loading resistance is also an order of magnitude larger than for any other antenna configuration.

V. Summary

We have seen that the role of capacitive coupling from the antenna is in general a non-negligible effect and should be considered as an important part of any power calculations. In addition, depending on the antenna geometry, this coupling can have a large affect on the observed light emission from the plasma. The inductive component of the antenna apparently couples to a symmetric, centrally peaked plasma. Antenna configurations which produced the highest density plasmas were numerically calculated to have the highest antenna loading, with the $m = +1$ configuration having the largest loading and producing the longest, brightest plasma. This strongly supports the notion that the helicon waves are not simply incidental in a high density discharge but are responsible for producing the discharge.

VI. ACKNOWLEDGMENTS

This work was supported by the National Science Foundation, Grant No. ECS-9400849, the Semiconductor Research Corporation, Project No. IJ-529, and the Wisconsin Engineering Center for Plasma-Aided Manufacturing. We thank Prof. Donald Arnush for considerable help with the interpretation of the results.

REFERENCES

1. Boswell R W 1984 *Plasma Phys Control Fusion* **26** 1147
2. Boswell R W, Porteus R K, Prytz A, Bouchoule A, and Ranson P 1982 *Phys Lett A* **91** 163
3. Chen F F and Chevalier G 1992 *J Vac Sci Technol A* **10** 1389
4. Komori A, Shoji T, Miyamoto K, Kawai J, and Kawai Y 1991 *Phys Fluids B* **3** 893
5. Degeling A W, Jung C O, Boswell R W, and Ellingboe A R 1996 *Phys Plasmas* **3** 2788
6. Light M and Chen F F 1995 *Phys Plasmas* **2** 1084
7. Shoji T, Sakawa Y, Nakazawa S, Kadota K, and Sato T 1993 *Plasma Sources Sci Technol* **2** 5
8. Davies B J 1970 *J Plasma Phys* **4** 43

9 Woods L C 1962 *J Fluid Mech* **13** 570

10 Ellingboe A R and Boswell R W 1996 *Phys Plasmas* **3** 2797

11 Chevalier G and Chen F F 1993 *J Vac Sci Technol A* **11** 1165

12 Fischer B, Kraemer M, and Enk Th, 1994 *Plasma Phys Control Fusion* **36** 2003

13 Shamrai K P and Taranov B V 1996 *Plasma Sources Sci Technol* **5** 474

14 Kamenski I V and Borg G G 1996 *Phys Plasmas* **3** 4396

15 Arnush D and Chen F F 1997 UCLA PPG-1573 submitted to *Phys Plasmas*

16 Kim J H, Yun S M and Chang H Y 1996 *IEEE Trans Plasma Sci* **24** 1364

17 Savas S E and Donohoe, K G 1989 Rev Sci Instrum **60** 3391

18 Sudit I D and Chen F F 1996 Plasma Sources Sci Technol **5** 43

19 Imre A I, Dashchenko A I, Zapesochnyi I P, and Kel'man V A 1972 JETP Lett **15** 503

20 Sudit I D and Chen F F 1994 Plasma Sources Sci Technol **3** 162

21. Blackwell D D and Chen F F 1996 Proc. SRC Techcon '96, Phoenix, Arizona (Semiconductor Research Corporation)

FIGURE CAPTIONS

1 Schematic of the apparatus showing the various positions of the CCD camera.

2 Geometry of the (a) Nagoya Type III and (b) helical antennas.

3 Argon plasma density at 3 mTorr with the Nagoya Type III antenna vs (a) RF power at 740 G and (b) magnetic field at 1.8 kW.

4 CCD images of the cross section of the plasma produced by the Nagoya Type III antenna Each contour denotes a 10% decrease in intensity. At approximately 500 G magnetic field, the plasma density jumps abruptly as the transition from a predominantly capacitively coupled discharge to a partially inductively coupled one occurs. Immediately before the jump (a), most of the light is concentrated near the antenna legs, whose positions are shown by the triangles. After the jump (b), plasma is created in the center of the chamber but is still asymmetric due to the influence of the antenna's electrostatic field. However, the onset of strong inductive coupling increases the light intensity by approximately a factor of two.

5 The plasma cross section for the Nagoya Type III antenna at 740 G and 1.8 kW of power, showing an elongation of the profile from top to bottom corresponding to the positions of the antenna wires.

6 Geometry of the Faraday shield used to eliminate capacitive coupling from the antenna The two sections have been separated in the drawing for clarity.

7 Same as Fig. 5, but with the Faraday shield installed. With the capacitive coupling eliminated, the plasma profile is nearly symmetric.

8 Plasma density with the shielded Nagoya Type III antenna vs. (a) RF power and (b) magnetic field. Conditions same as in Fig. 3.

9 End view of the plasma in the low-power, low-density regime prior to the onset of helicon wave coupling at the density jump in Fig. 8a.

10 Plasma density with the helical antenna vs. (a) RF power and (b) magnetic field. The magnetic field and the antenna helicity combine to excite an m = +1 azimuthal mode Other conditions same as in Fig. 3.

11 Ar^+ emission profile of the plasma produced by the helical antenna at 740 G, 1.8 kW, and 3 mTorr. A 10% filter was used, since the emission intensity in this image is 50× higher than with the Nagoya antenna under the same conditions (Fig. 5).

12 Plasma density with the helical antenna, with and without the Faraday shield, vs. (a) RF power and (b) magnetic field strength. Conditions same as in Fig. 3.

13 Transverse image of the discharge at 740 G for the three antenna configurations: (a) Nagoya Type III, (b) left-handed helical, and (c) right-handed helical. The numbers shown correspond to the three camera positions in Fig. 1. The brightest and longest plasma (c) corresponds to the m = +1 azimuthal mode.

14 The k-spectra of the antenna current J_φ for the helical and Nagoya Type III antennas.

15 The k-spectra of antenna loading resistance calculated for both types of antennas with a mean plasma radius of approximately 3 cm, a peak density of 3×10^{13} cm^{-3}, and a magnetic field of 800 G. The helical antenna spectrum is seen to be asymmetric with much higher loading than for the Nagoya Type III antenna.

16. Cross section for excitation of the 488-nm line in e-Ar^+ collisions as a function of electron energy.

17. Computed variation of the probability of exciting the 488-nm line from Ar^+ due to changes in electron temperature (dashed line) and changes in density (solid line). The expected range of T_e in the experiment is shown by the shaded portion of the dashed line, while the range of densities in the experiment covers the entire graph.

18. Radial profiles of electron temperature in similar helicon discharges studied earlier.

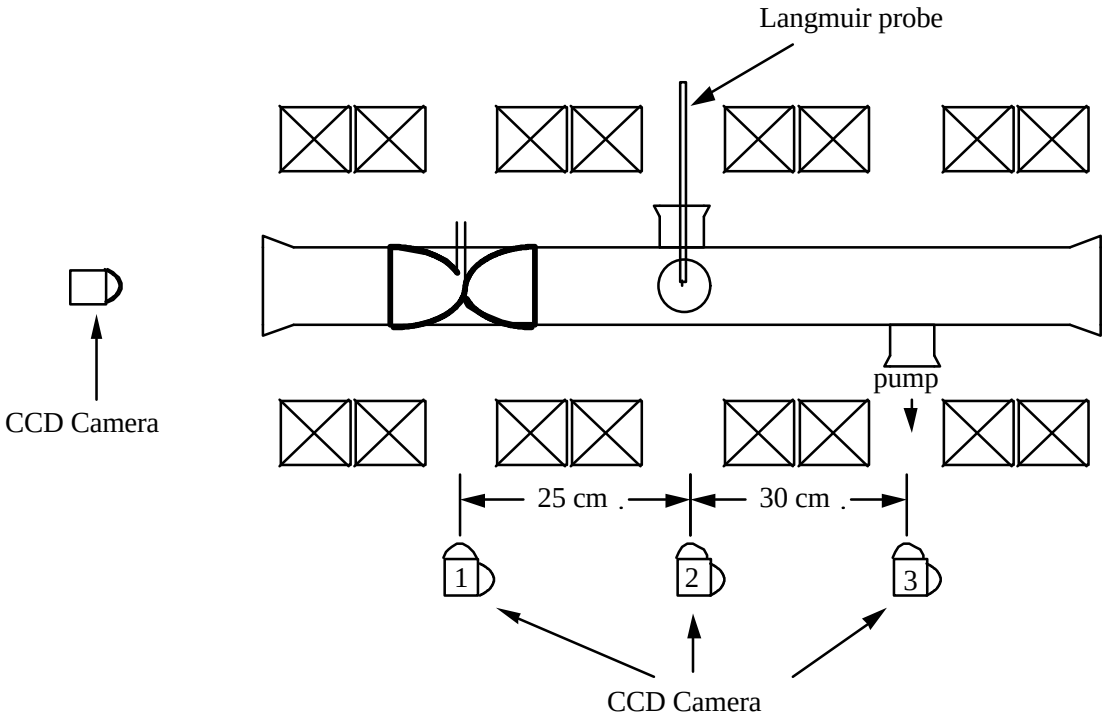

Fig. 1

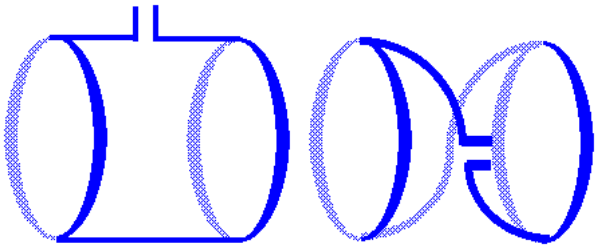

(a) Fig. 2 (b)

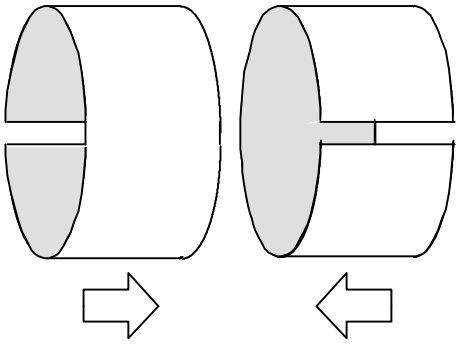

Fig. 6

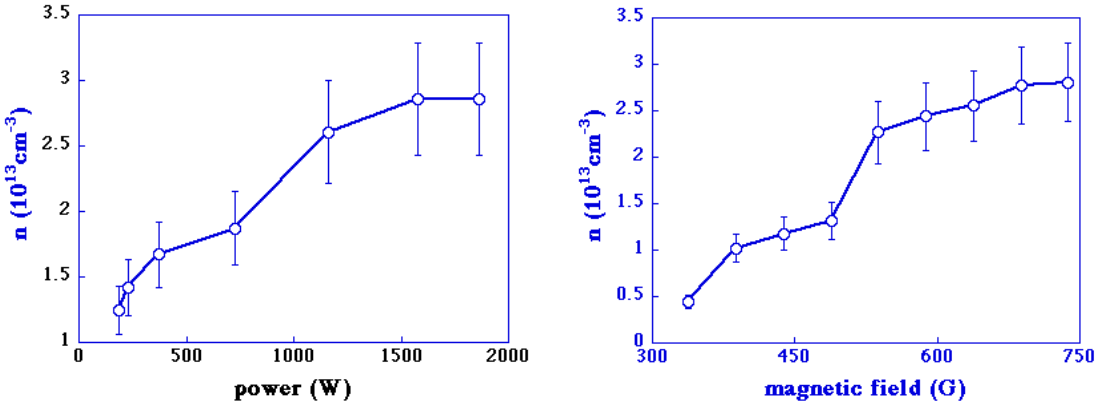

(a) (b)

Fig. 3

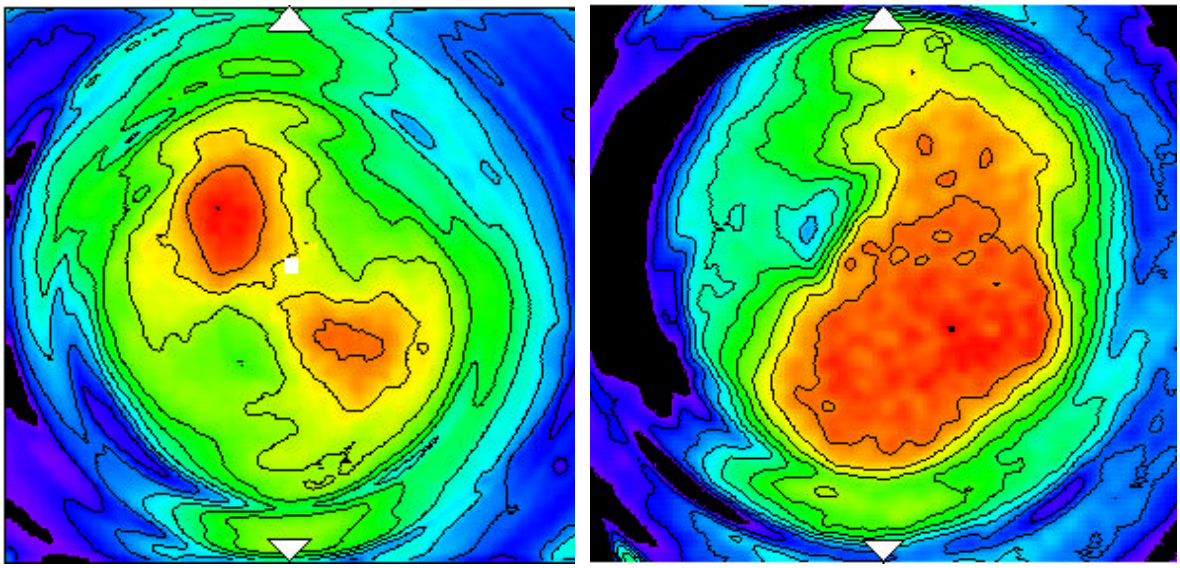

(a) (b)

Fig. 4

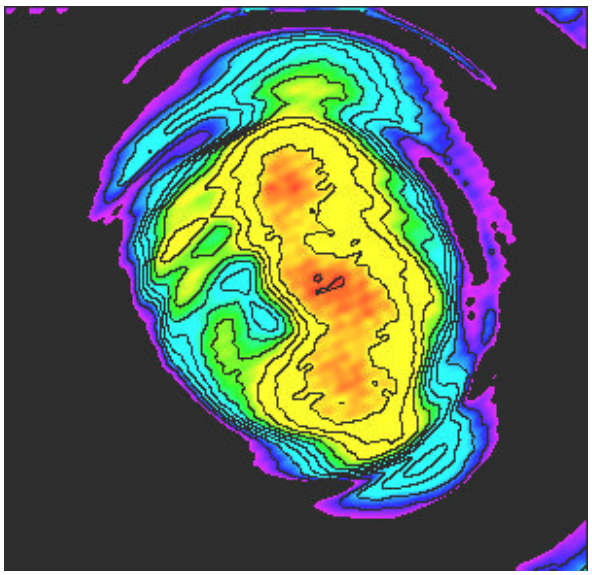

Fig. 5

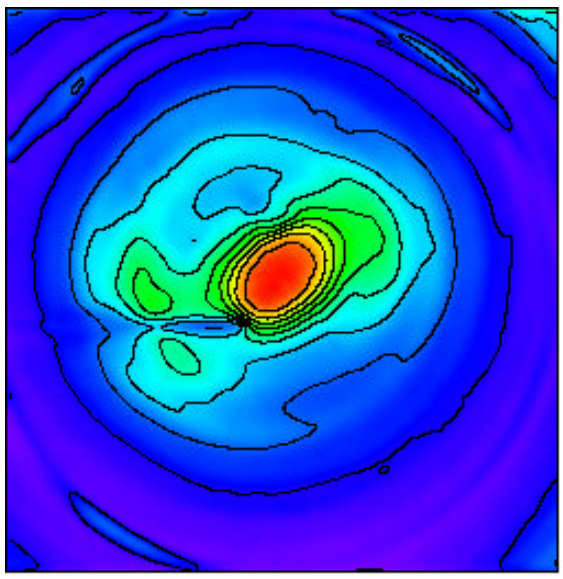

Fig. 7

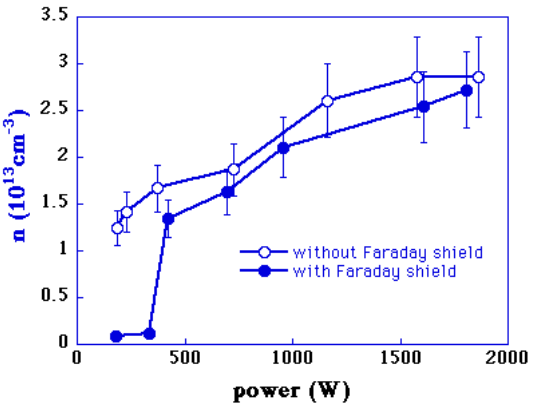

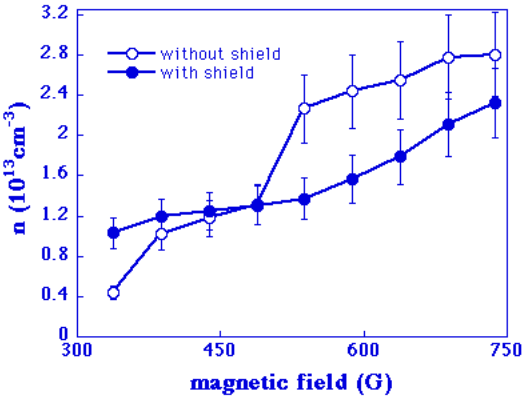

(a) Fig. 8 (b)

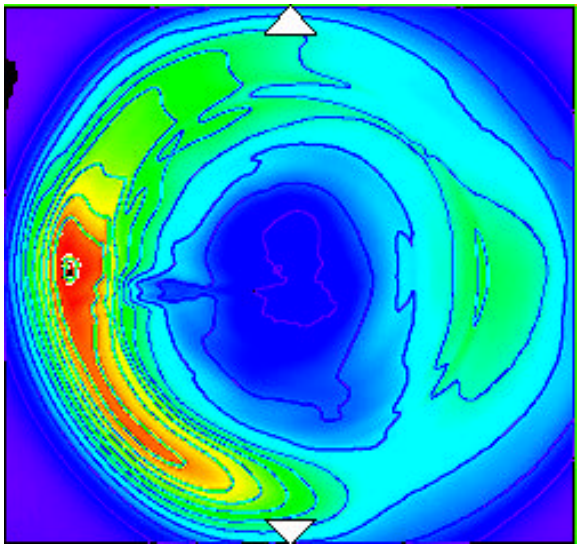

Fig. 9

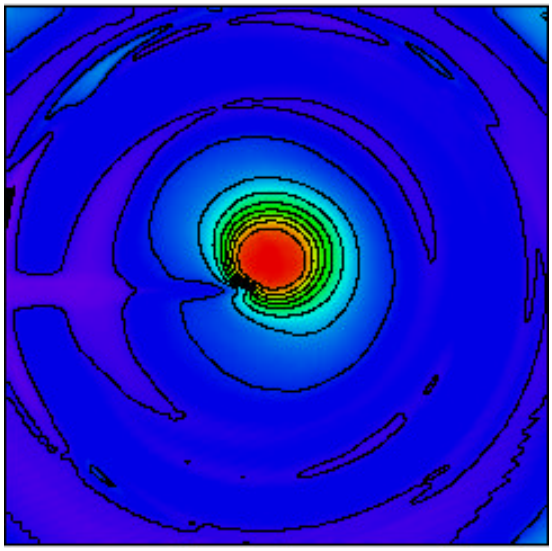

Fig. 11

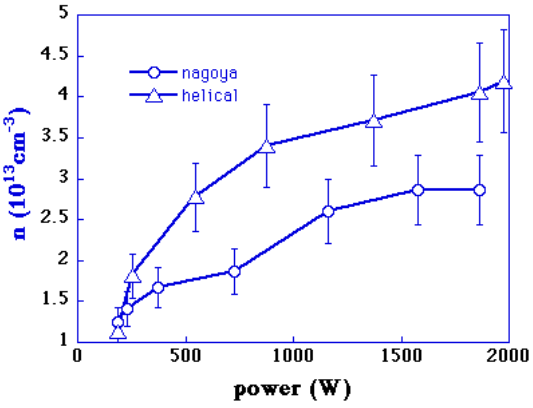

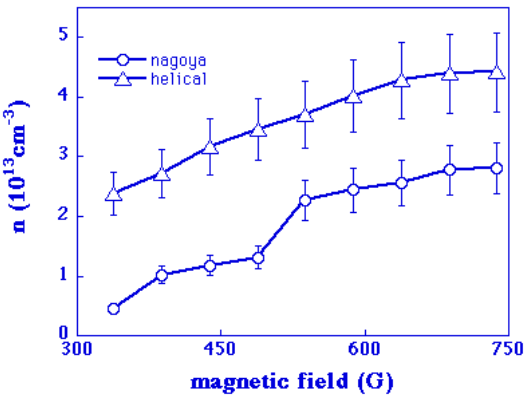

(a) Fig. 10 (b)

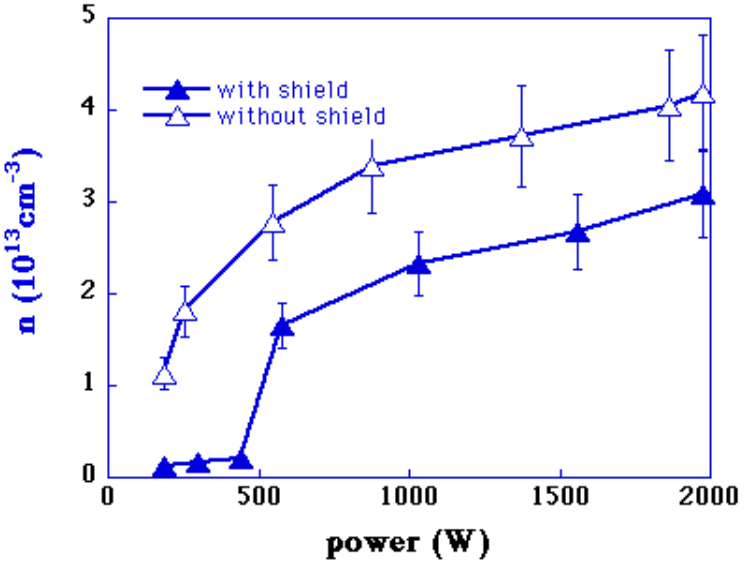

(a)

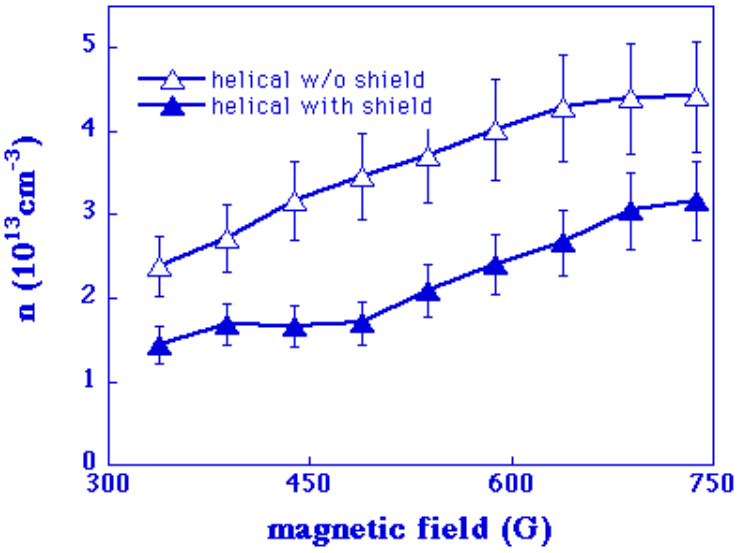

(b)

Fig. 12

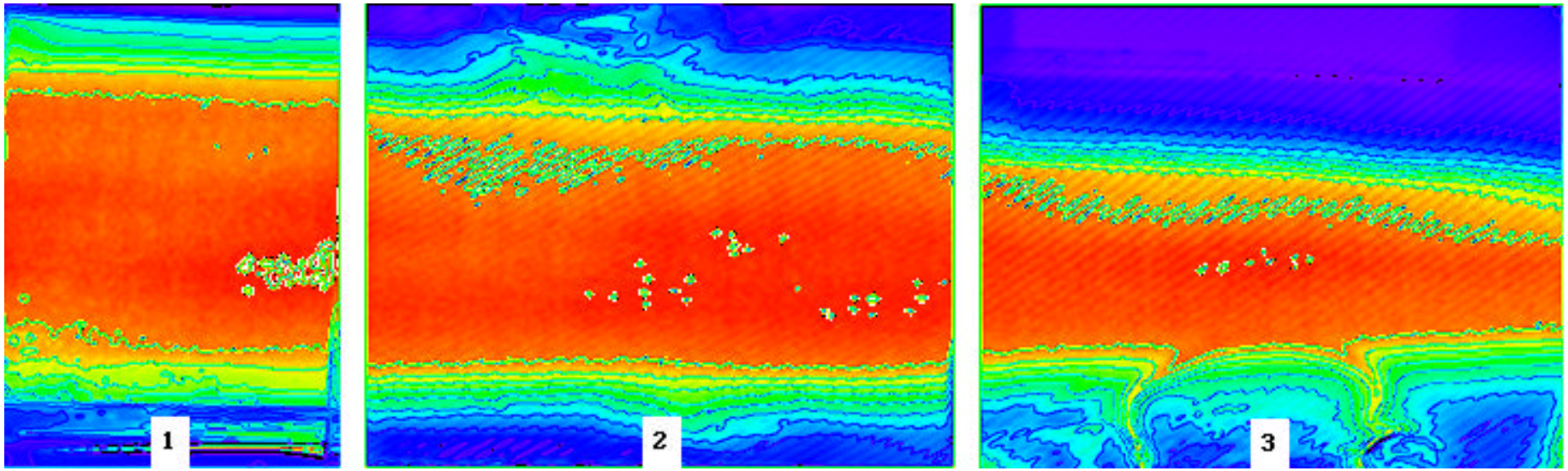

Fig. 13a

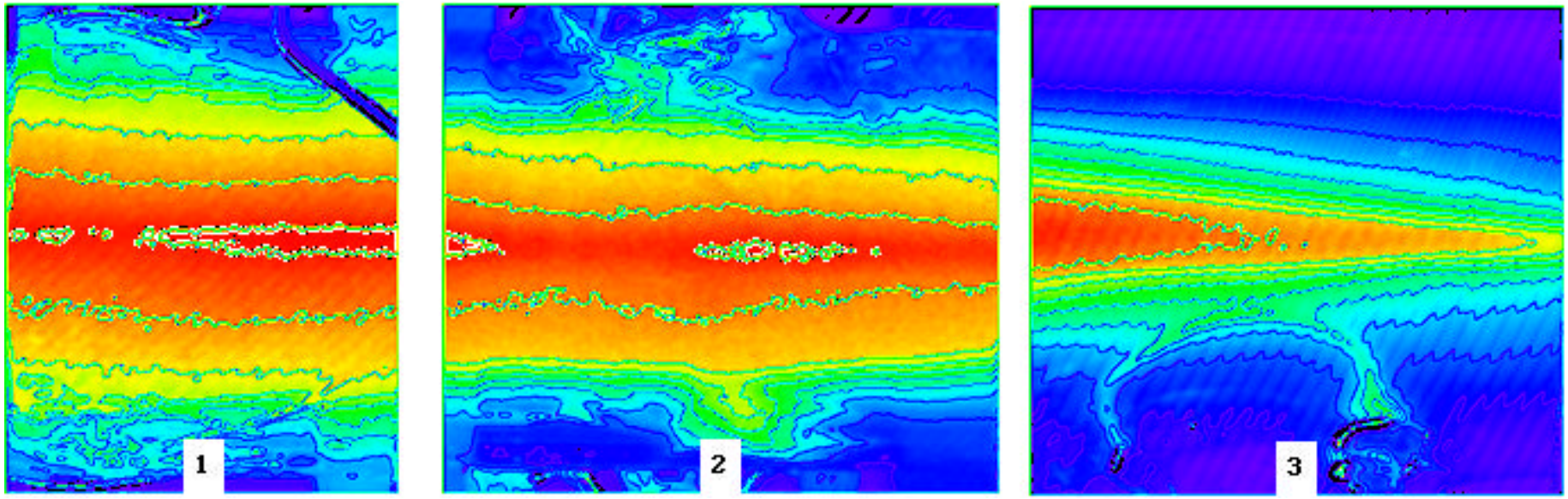

Fig. 13b

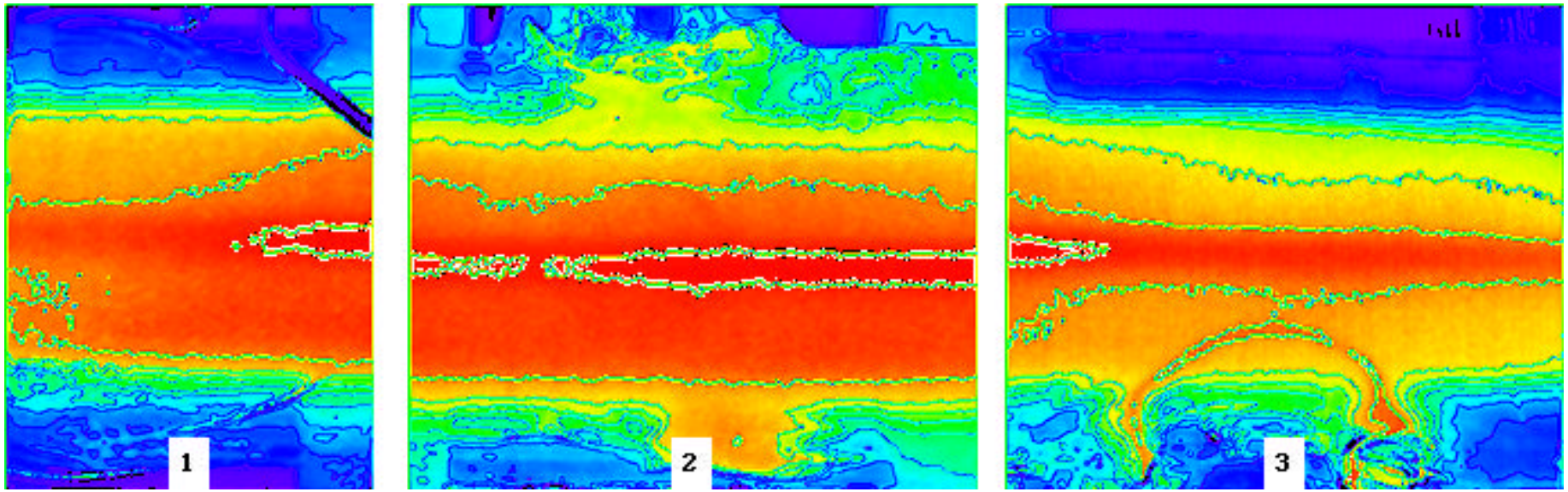

Fig. 13c

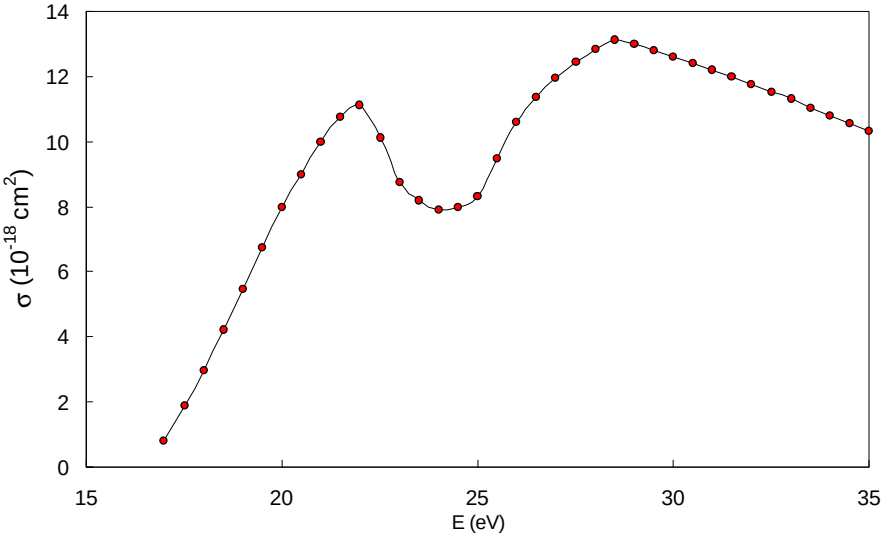
σ (10^-18 cm^2)
E (eV)

Fig. 14

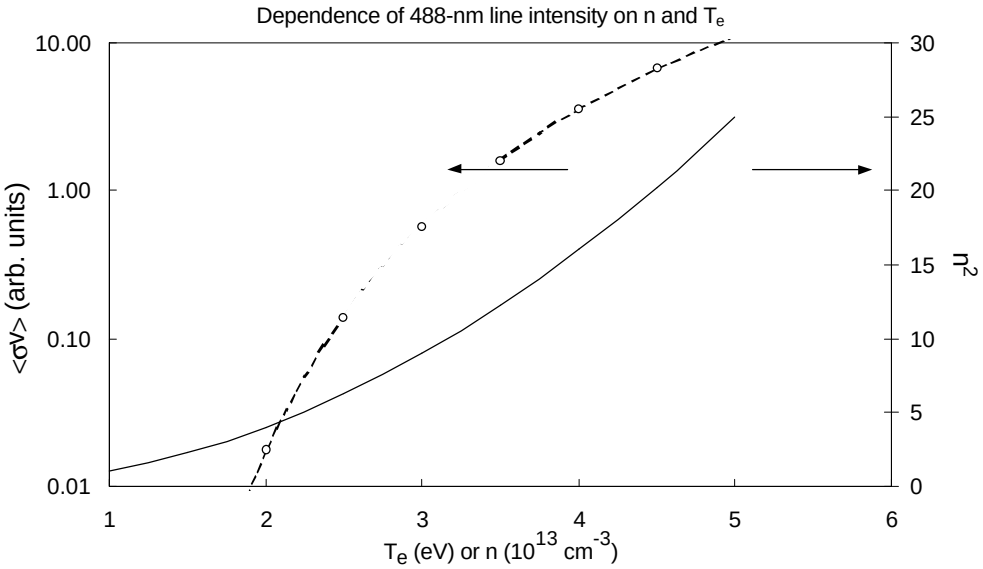
Dependence of 488-nm line intensity on n and Te
<σv> (arb. units)
n^2
Te (eV) or n (10^13 cm^-3)

Fig. 15

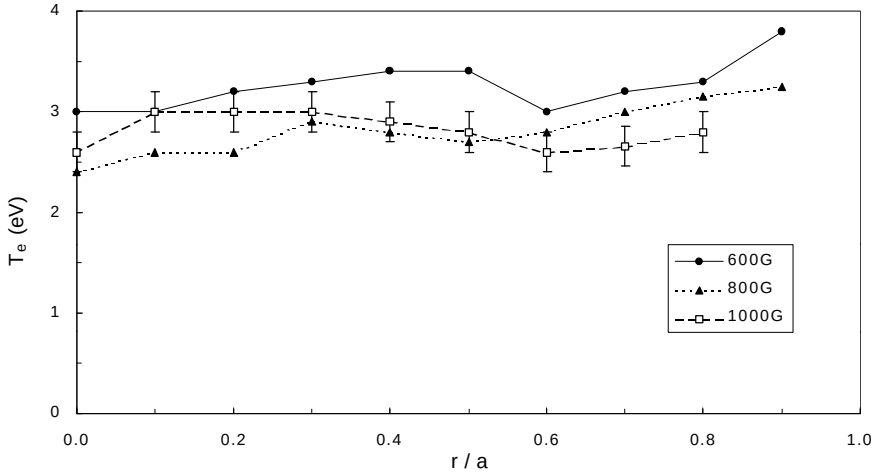
Te (eV)
r / a
600G
800G
1000G

Fig. 16

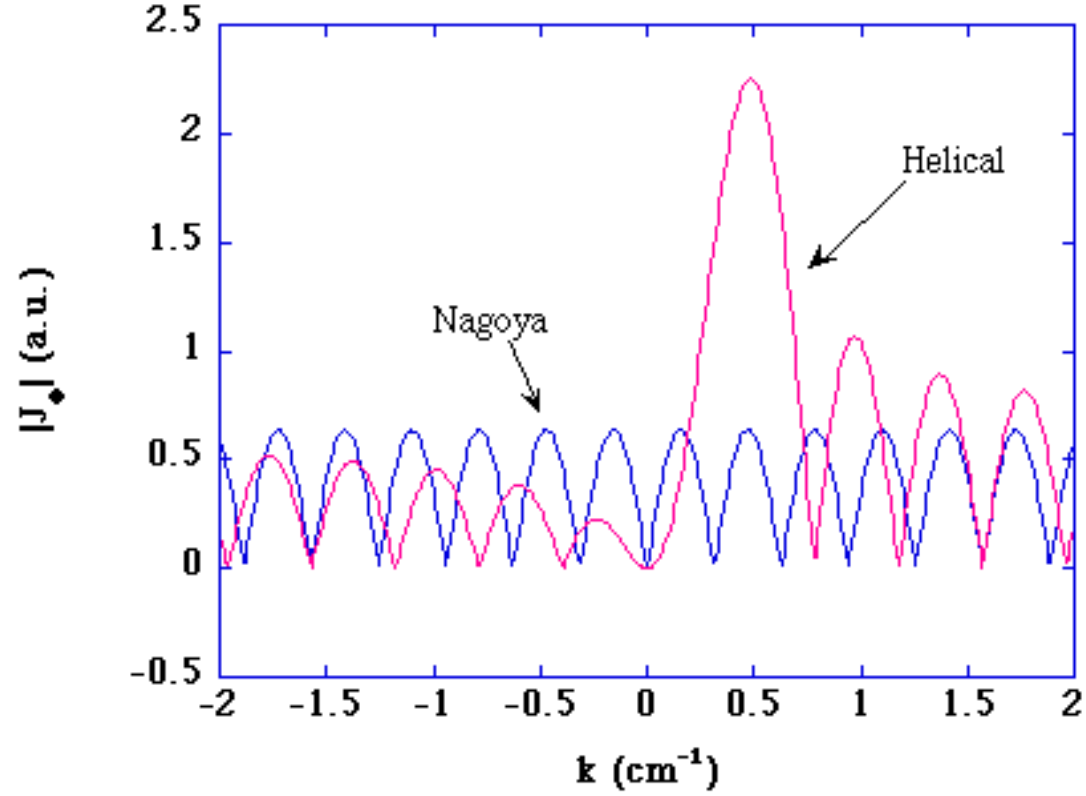

Fig. 17

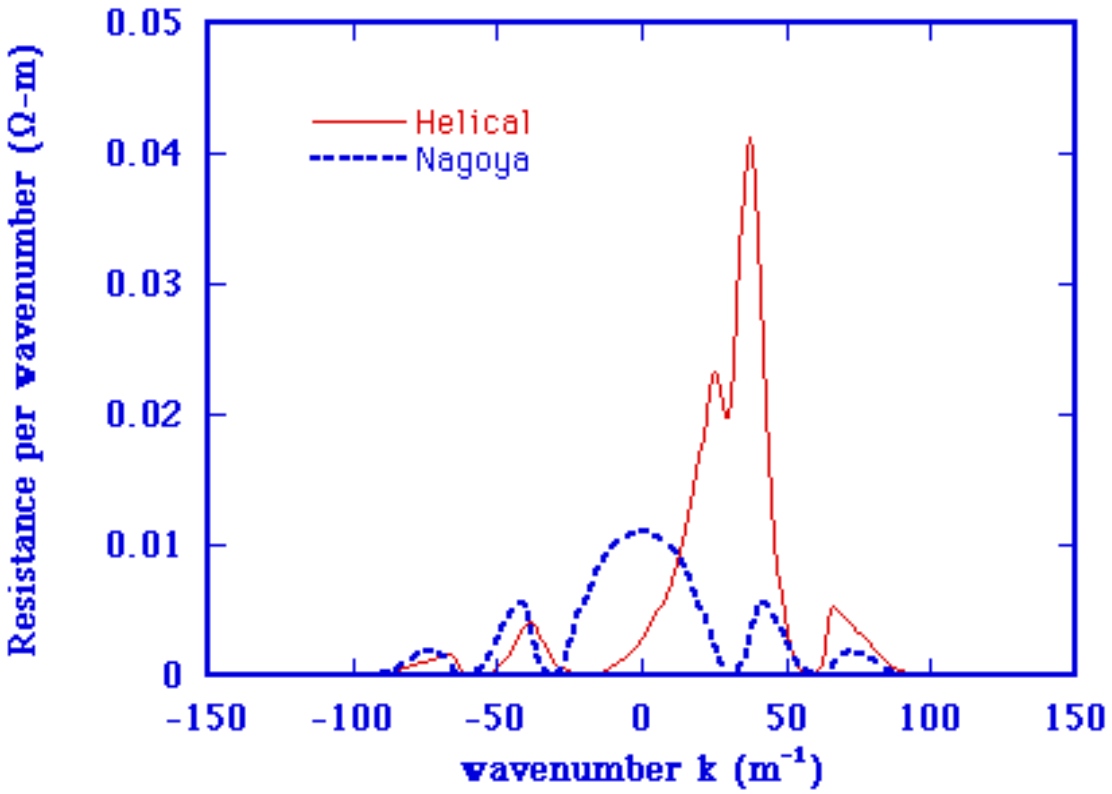

Fig. 18